

Charmonium decays to $\gamma\pi^0$, $\gamma\eta$, and $\gamma\eta'$

T. K. Pedlar,¹ J. Xavier,¹ D. Cronin-Hennessy,² K. Y. Gao,² J. Hietala,² T. Klein,²
 R. Poling,² P. Zweber,² S. Dobbs,³ Z. Metreveli,³ K. K. Seth,³ B. J. Y. Tan,³
 A. Tomaradze,³ J. Libby,⁴ L. Martin,⁴ A. Powell,⁴ C. Thomas,⁴ G. Wilkinson,⁴
 H. Mendez,⁵ J. Y. Ge,⁶ D. H. Miller,⁶ I. P. J. Shipsey,⁶ B. Xin,⁶ G. S. Adams,⁷ D. Hu,⁷
 B. Moziak,⁷ J. Napolitano,⁷ K. M. Ecklund,⁸ Q. He,⁹ J. Insler,⁹ H. Muramatsu,⁹
 C. S. Park,⁹ E. H. Thorndike,⁹ F. Yang,⁹ M. Artuso,¹⁰ S. Blusk,¹⁰ S. Khalil,¹⁰
 R. Mountain,¹⁰ K. Randrianarivony,¹⁰ T. Skwarnicki,¹⁰ S. Stone,¹⁰ J. C. Wang,¹⁰
 L. M. Zhang,¹⁰ G. Bonvicini,¹¹ D. Cinabro,¹¹ M. Dubrovin,¹¹ A. Lincoln,¹¹ M. J. Smith,¹¹
 P. Zhou,¹¹ J. Zhu,¹¹ P. Naik,¹² J. Rademacker,¹² D. M. Asner,¹³ K. W. Edwards,¹³
 J. Reed,¹³ A. N. Robichaud,¹³ G. Tatishvili,¹³ E. J. White,¹³ R. A. Briere,¹⁴ H. Vogel,¹⁴
 P. U. E. Onyisi,¹⁵ J. L. Rosner,¹⁵ J. P. Alexander,¹⁶ D. G. Cassel,¹⁶ R. Ehrlich,¹⁶
 L. Fields,¹⁶ R. S. Galik,¹⁶ L. Gibbons,¹⁶ R. Gray,¹⁶ S. W. Gray,¹⁶ D. L. Hartill,¹⁶
 B. K. Heltsley,¹⁶ D. Hertz,¹⁶ J. M. Hunt,¹⁶ J. Kandaswamy,¹⁶ D. L. Kreinick,¹⁶
 V. E. Kuznetsov,¹⁶ J. Ledoux,¹⁶ H. Mahlke-Krüger,¹⁶ J. R. Patterson,¹⁶ D. Peterson,¹⁶
 D. Riley,¹⁶ A. Ryd,¹⁶ A. J. Sadoff,¹⁶ X. Shi,¹⁶ S. Stroiney,¹⁶ W. M. Sun,¹⁶ T. Wilksen,¹⁶
 J. Yelton,¹⁷ P. Rubin,¹⁸ N. Lowrey,¹⁹ S. Mehrabyan,¹⁹ M. Selen,¹⁹ J. Wiss,¹⁹
 M. Kornicer,²⁰ R. E. Mitchell,²⁰ M. R. Shepherd,²⁰ C. Tarbert,²⁰ and D. Besson²¹

(CLEO Collaboration)

¹Luther College, Decorah, Iowa 52101, USA

²University of Minnesota, Minneapolis, Minnesota 55455, USA

³Northwestern University, Evanston, Illinois 60208, USA

⁴University of Oxford, Oxford OX1 3RH, UK

⁵University of Puerto Rico, Mayaguez, Puerto Rico 00681

⁶Purdue University, West Lafayette, Indiana 47907, USA

⁷Rensselaer Polytechnic Institute, Troy, New York 12180, USA

⁸Rice University, Houston, TX 77005, USA

⁹University of Rochester, Rochester, New York 14627, USA

¹⁰Syracuse University, Syracuse, New York 13244, USA

¹¹Wayne State University, Detroit, Michigan 48202, USA

¹²University of Bristol, Bristol BS8 1TL, UK

¹³Carleton University, Ottawa, Ontario, Canada K1S 5B6

¹⁴Carnegie Mellon University, Pittsburgh, Pennsylvania 15213, USA

¹⁵Enrico Fermi Institute, University of Chicago, Chicago, Illinois 60637, USA

¹⁶Cornell University, Ithaca, New York 14853, USA

¹⁷University of Florida, Gainesville, Florida 32611, USA

¹⁸George Mason University, Fairfax, Virginia 22030, USA

¹⁹University of Illinois, Urbana-Champaign, Illinois 61801, USA

²⁰Indiana University, Bloomington, Indiana 47405, USA

²¹University of Kansas, Lawrence, Kansas 66045, USA

(Dated: April 8, 2009)

Abstract

Using data acquired with the CLEO-c detector at the CESR e^+e^- collider, we measure branching fractions for J/ψ , $\psi(2S)$, and $\psi(3770)$ decays to $\gamma\pi^0$, $\gamma\eta$, and $\gamma\eta'$. Defining $R_n \equiv \mathcal{B}[\psi(nS) \rightarrow \gamma\eta]/\mathcal{B}[\psi(nS) \rightarrow \gamma\eta']$, we obtain $R_1 = (21.1 \pm 0.9)\%$ and, unexpectedly, an order of magnitude smaller limit, $R_2 < 1.8\%$ at 90% C.L. We also use $J/\psi \rightarrow \gamma\eta'$ events to determine branching fractions of improved precision for the five most copious η' decay modes.

PACS numbers: 13.20.Gd,13.20.Jf

In the conventional view of quantum chromodynamics (QCD), the mass eigenstates J/ψ , $\psi(2S)$, and $\psi(3770)$ represent the $1S$, $2S$, and $1D$ $c\bar{c}$ states, respectively (with some evidence of modest $2S-1D$ mixing [1]). Most hadronic decays of these states that are not transitions to lower-lying charmonia or decays to open charm can be described at tree level by $c\bar{c}$ annihilation into either three gluons (ggg) or a photon plus two gluons (γgg). However, some final states can be reached by less common routes, and their study can lend experimental constraints on the relevant QCD predictions. In this article we describe measurements of branching fractions for each of J/ψ , $\psi(2S)$, and $\psi(3770)$ decays to three such final states: $\gamma\pi^0$, $\gamma\eta$, and $\gamma\eta'$. In the $b\bar{b}$ system, limits of $\mathcal{B}(\Upsilon(1S) \rightarrow \gamma\eta^{(\prime)}) < 1.0(1.9) \times 10^{-6}$ have been set [2] and are smaller than expected. Comparable studies in the charmonium sector are warranted.

Vector charmonium decays to a photon and a light pseudoscalar ($\psi(nS) \rightarrow \gamma P$) can be described by a variety of mechanisms at the parton level, which we label $(i)-(vi)$. When $P = \eta$ or η' , the primary source is generally thought to be (i) $\psi(nS) \rightarrow \gamma gg$, which then fragments to exclusive final states in a flavor-blind manner. The η and η' mesons are commonly understood as mixtures of the pure SU(3)-flavor octet $[(u\bar{u} + d\bar{d} - 2s\bar{s})/\sqrt{6}]$ and singlet $[(u\bar{u} + d\bar{d} + s\bar{s})/\sqrt{3}]$ states and a small gluonium component [3, 4]. The flavor content of each $\eta^{(\prime)}$ mass eigenstate can be quantified with a mixing angle, the value of which becomes manifest in ratios of branching fractions for various radiative decays involving an η or η' [5, 6, 7]. Under the assumption that all $\psi(nS) \rightarrow \gamma\eta^{(\prime)}$ final states occur through (i) , the $\eta-\eta'$ mixing angle can be extracted from a measurement of $R_n \equiv \mathcal{B}[\psi(nS) \rightarrow \gamma\eta]/\mathcal{B}[\psi(nS) \rightarrow \gamma\eta']$ and compared with values obtained from other decays [5, 8].

Alternate $c\bar{c}$ annihilation mechanisms for γP final states are mediated either by three gluons or a virtual photon: (ii) $\psi(nS) \rightarrow ggg \rightarrow q\bar{q}\gamma_{\text{fsr}}$ (where γ_{fsr} represents final state radiation off one of the quarks) or (iii) $\psi(nS) \rightarrow \gamma^* \rightarrow q\bar{q}\gamma_{\text{fsr}}$. It has also been suggested that an M1 transition to η_c followed by $\eta_c-\eta^{(\prime)}$ mixing [9, 10] (iv) $\psi(nS) \rightarrow \gamma\eta_c^* \rightarrow \gamma\eta^{(\prime)}$ could contribute. The vector dominance model (VDM) can be used to predict [11] (v) $\psi(2S) \rightarrow J/\psi^*\eta \rightarrow \gamma\eta$. For all these processes $R_1 \approx R_2$ is expected. Previous measurements [12] yield $R_1 = (20.8 \pm 2.4)\%$, consistent with the dominance of (i) with an $\eta-\eta'$ mixing angle in the expected range [12]. However, rate determinations for $\psi(2S)$ decays have yielded $R_2 < 66\%$ at 90% confidence level (C.L.) [12] and hence are not yet precise enough to confirm a value comparable to R_1 . No measurements for $\psi(3770) \rightarrow \gamma\eta^{(\prime)}$ have yet been reported.

When $P = \pi^0$, processes (i) and (iv) violate isospin conservation, and are therefore suppressed relative to process (iii) or (v) above, or (vi) $ggg \rightarrow 2(q\bar{q}) \rightarrow \rho^{0*}\pi^0$, $\rho^{0*} \rightarrow \gamma$ via VDM. Ref. [13] (CZ) finds process (ii) to be negligible, but (iii) and (vi) to be of comparable magnitude and fully coherent. Updating the CZ VDM calculation to current experimental branching fractions and widths [12] gives $\mathcal{B}(J/\psi \rightarrow \gamma\pi^0) \approx 6 \times 10^{-5}$, nearly double the PDG average measurement of $(3.3_{-0.4}^{+0.6}) \times 10^{-5}$ [12]. A similar disparity was measured in Ref. [14] for $\gamma^*\gamma \rightarrow \pi^0$ for spacelike non-asymptotic momentum transfers in the range $|q^2| = 1.5 - 9$ GeV², where the CZ prediction was found to significantly overshoot the data. Further experimental precision on $\mathcal{B}(J/\psi \rightarrow \gamma\pi^0)$ would allow a more precise indirect measurement of the $\gamma^* - \gamma\pi^0$ vertex of process (iii) for timelike photons [15].

For this measurement, events were acquired at the CESR e^+e^- collider with the CLEO detector [16], mostly in the CLEO-c configuration (5% of $\psi(2S)$ data were collected with CLEO III). The data samples comprise $(27.4 \pm 0.6) \times 10^6$ [17] produced $\psi(2S)$ mesons, of which $(9.589 \pm 0.020 \pm 0.070) \times 10^6$ [17] decay into $\pi^+\pi^-J/\psi$ (our source for J/ψ decays), and 814 pb^{-1} at $\sqrt{s} = 3.773$ GeV, corresponding to $(5.3 \pm 0.1) \times 10^6$ [18] produced $\psi(3770)$

mesons. We also utilize 20.7 pb^{-1} of data taken at $\sqrt{s} = 3.671 \text{ GeV}$, just below the $\psi(2S)$ peak, for a “continuum” subtraction of backgrounds.

We select events in the decay modes shown in Table I; modes that are not shown have sensitivity inferior to those we employ. Every particle in each mode’s decay chain must be found. Each such particle is constrained to originate from a single point (vertex) consistent with the measured beam spot. We then constrain the sum of all four-momenta to the known $\psi(2S)$ mass [12] and initial e^+e^- three-momentum. The vertex and full event four-momentum kinematic fits must satisfy quality requirements of $\chi_V^2/\text{d.o.f.} < 10$ and $\chi_E^2/\text{d.o.f.} < 10$, respectively, which typically retain 90-99% of signal events. For $\psi(2S) \rightarrow \gamma\pi^0$, tighter restrictions of $\chi_V^2/\text{d.o.f.} < 3$ and $\chi_E^2/\text{d.o.f.} < 3$ suppress QED background. Further selections are based on four-momenta from the fit.

Masses of final state or intermediate mesons must be found in the signal or sideband windows given in Table II. Note that different windows apply depending on the $\eta^{(\prime)}$ decay mode because mass resolution depends upon the final state. The tracking system must find zero, two, or four tracks of net charge zero for the $\pi^0/\eta/\eta'$ decay products, and, for J/ψ modes, exactly two additional oppositely-charged particles for the $\psi(2S)$ -to- J/ψ -transition. Photon candidate showers must lie in the barrel region of the calorimeter ($|\cos\theta| < 0.75$) where the energy resolution and finding-efficiency are most favorable and well-modeled. Photon candidates must also have energy $E_\gamma > 37 \text{ MeV}$, lie more than 30 cm from the center of any shower associated with one of the charged pions, and not align with the initial three-momentum of any π^\pm candidate within 100 mrad. A photon candidate is included in the decay chain only if all more energetic ones are also used. Photon pairs from π^0 or η are constrained to the appropriate mass [12], except in $\eta \rightarrow 3\pi^0$ and $\eta' \rightarrow \pi^0\pi^0\eta(\gamma\gamma)$; these final states are only required to have six photons with a combined invariant mass in the corresponding mass window in Table II. Photons in $\eta^{(\prime)} \rightarrow \gamma\pi^+\pi^-$ and $\eta' \rightarrow \pi^+\pi^-\eta(\gamma\pi^+\pi^-)$ must have $E_\gamma > 100 \text{ MeV}$ to suppress feedacross from other η and η' decays; photons in $\psi(2S) \rightarrow \gamma\pi^0$ and $\psi(3770) \rightarrow \gamma\pi^0$ must have $E_\gamma > 300 \text{ MeV}$ to suppress $e^+e^- \rightarrow 3\gamma$.

For $\psi(3770)$ modes, where signal yields are expected to be small, backgrounds larger, and systematic considerations much less important, we take measures to enhance efficiency and suppress backgrounds at the expense of systematic precision. The photon-finding criteria are loosened so as to increase efficiency: barrel and endcap showers are used ($|\cos\theta| < 0.83$ or $0.85 < |\cos\theta| < 0.93$), and showers between 15 and 30 cm from a shower associated with a charged track are accepted if they have a photon-like lateral shape. In addition, the four-momentum constrained fit quality is tightened to $\chi_E^2/\text{d.o.f.} < 3$ to suppress backgrounds.

Efficiencies for signal and feedacross from other modes considered here are modeled with Monte Carlo (MC) samples that were generated using the EVTGEN event generator [19], fed through a GEANT-based [20] detector simulation, and subjected to the same event selection criteria as the data. We model $\eta \rightarrow \gamma\gamma$ and $3\pi^0$ as phase-space-like decays. The decay $\eta \rightarrow \gamma\pi^+\pi^-$ is simulated as mediated by a $\rho^0 \rightarrow \pi^+\pi^-$, weighted with a factor E_γ^3 , where E_γ is the photon energy in the η center-of-mass system, which results in the excellent agreement with the measured dipion mass distribution seen in Ref. [21]. The decay $\eta' \rightarrow \gamma\pi^+\pi^-$ is handled similarly, but using a factor of E_γ^2 , and MC-data agreement is shown in Ref. [22]. We generate $\eta \rightarrow \pi^+\pi^-\pi^0$ according to the distribution measured in Ref. [23]. All other η' decays are generated using phase space. For each decay mode, we try all combinations for assignment of the selected tracks and showers (although in practice more than a single successful one per event is rare).

We also tally an event satisfying the selections if instead of lying inside the light meson

signal mass window it has mass within one of the two sideband regions indicated in Table II. Similarly, the number of events with $\pi^+\pi^-$ recoil mass inside the sidebands is accumulated for each J/ψ mode. To allow for possible double-counting of non- J/ψ and light meson mass-sideband backgrounds, we only subtract half of the window-size-scaled dipion recoil mass sideband number for each mode, and assign a systematic uncertainty of the full scaled number.

We subtract feedacross attributable to any radiative J/ψ or $\psi(2S)$ decays into $\gamma\pi^0$, $\gamma\eta$, and $\gamma\eta'$, including the decay modes not selected. To do so, we employ MC samples that are normalized to the observed net yields and η' relative branching fractions found here, except for η , ω , and π^0 decay modes not probed, for which PDG [12] branching fractions are used. Continuum data counts satisfying the selections are subtracted after scaling by relative luminosity and $1/s$. The mass sideband subtraction is performed in the MC and continuum samples, assuring that the efficiency, feedacross, and continuum backgrounds are computed correctly. This procedure implicitly assumes that backgrounds other than from continuum and feedacross are linear in pseudoscalar candidate mass; it explicitly accounts for nonlinear backgrounds from continuum and feedacross.

Applying the above-described selection criteria to our data and MC samples yields the results shown in Table I, in which raw yields for signal and sidebands are given along with appropriately scaled feedacross and continuum corrections. The signal efficiency is also given for each mode, which ranges from 5% to 36%. All modes except $\psi(2S) \rightarrow \gamma\pi^0$ and $\psi(3770) \rightarrow \gamma\pi^0$ have very small backgrounds. No statistically significant signals are seen for $\psi(2S) \rightarrow \gamma\eta$, $\psi(2S) \rightarrow \gamma\pi^0$, or $\psi(3770) \rightarrow \gamma\pi^0$.

The light meson mass distributions for all modes are shown in Figs. 1-4; plots for J/ψ (other) modes have logarithmic (linear) vertical scales. Background from $e^+e^- \rightarrow 3\gamma$ that contaminates $\psi(2S) \rightarrow \gamma\pi^0$ and $\psi(3770) \rightarrow \gamma\pi^0$, visible in Figs. 1(b) and 4(a), respectively, is irregular in shape but modeled well by the scaled continuum data. There is also a nonlinear background shape for modes involving $\eta \rightarrow \gamma\pi^+\pi^-$ decays, but it is well-modeled by the MC as it is due to feedacross from $\eta \rightarrow \pi^+\pi^-\pi^0$. A typical $\psi(2S)$ -to- J/ψ -transition dipion recoil mass distribution appears in Ref. [22], showing a tiny and flat non- J/ψ background; this is typical of all modes. Ample signals for $J/\psi \rightarrow \gamma\pi^0$, $J/\psi \rightarrow \gamma\eta$, $J/\psi \rightarrow \gamma\eta'$, and $\psi(2S) \rightarrow \gamma\eta'$ are apparent and well-modeled by the MC-predicted shapes, aside from very small backgrounds that are approximately linear in mass.

We make the first observations of $e^+e^- \rightarrow \gamma\eta^{(\prime)}$ at $\sqrt{s} = 3.773$ GeV with statistical significances of $5.0(6.4)\sigma$ and observed cross sections $(0.17_{-0.04}^{+0.05} \pm 0.03)$ pb ($\gamma\eta$) and $(0.21_{-0.05}^{+0.07} \pm 0.03)$ pb ($\gamma\eta'$). The fraction of these values attributable to continuum cannot be estimated accurately from our $\sqrt{s} = 3.671$ GeV dataset due to its relatively small size: zero observed $\gamma\eta^{(\prime)}$ events yields upper limits at 90% C.L. of < 2 pb for both processes. However, continuum cross sections for $e^+e^- \rightarrow \gamma\eta^{(\prime)}$ at $\sqrt{s} = 10.58$ GeV have been measured by BABAR [24] to be $4.5_{-1.1}^{+1.2} \pm 0.3$ ($5.4 \pm 0.8 \pm 0.3$) fb. Extrapolating [15] to the charmonium energy region requires knowledge of the q^2 dependence of the form factors [25] $F_{\eta^{(\prime)}}(q^2)$ for $\gamma^* \rightarrow \gamma\eta^{(\prime)}$. According to CLEO measurements [14] of the $\gamma\gamma^* \rightarrow \eta^{(\prime)}$ spacelike form factors, $|q^2 F_{\eta^{(\prime)}}(q^2)|$ is 15 ± 10 (5 ± 5)% smaller than that at $q^2 = m^2[\Upsilon(4S)]$ for q^2 in the charmonium region. Continuum cross sections for $e^+e^- \rightarrow \gamma\eta^{(\prime)}$ are expected [25] to scale as $|F_{\eta^{(\prime)}}(q^2)|^2$, leading to an estimate of 0.19 ± 0.07 (0.25 ± 0.05) pb at $\sqrt{s} = 3.773$ GeV. These levels indicate a dominant continuum component in our signals. Other potential sources of background for the $\psi(3770)$ data sample are decays from the tail of the $\psi(2S)$, $e^+e^- \rightarrow \psi(2S) \rightarrow \gamma P$ at $\sqrt{s} = 3.773$ GeV, and radiative returns (rr) to the peak of the

$\psi(2S)$, $e^+e^- \rightarrow \gamma_{\text{rr}}\psi(2S) \rightarrow \gamma_{\text{rr}}\gamma P$. Using the methods of Ref. [26], these contributions are estimated to be negligible: the former due to its inherently small rate and the latter because such events will fail the kinematic selections due to the presence of γ_{rr} .

Notable in Fig. 2(c), 2(e), and 2(g) is the absence of any $\psi(2S) \rightarrow \gamma\eta$ signal; we set an upper limit on the cross section at $\sqrt{s} = 3.686$ GeV of < 1.1 pb, about one tenth of that expected if $R_2 = R_1$ were true. We can rule out destructive interference with a continuum $\gamma\eta$ signal as the primary cause of the deficit because, as discussed above, the continuum cross section is too small.

The statistical errors on efficiencies and subtractions for sideband, feedacross, and continuum are combined with the statistical uncertainties on event counts in the data. For systematic uncertainties associated with finding tracks and showers, we assign 0.3% per track and 0.4% per photon [17] on a mode-by-mode basis, accounting for correlations in such uncertainties in arithmetic computations involving two or more modes. For the looser photon criteria applied to $\psi(3770)$ modes, a larger uncertainty of 3% per photon is assigned. Systematic uncertainties of 1% (relative) are assigned to efficiencies, uncorrelated mode-to-mode, and account for any dataset or trigger modeling dependence. We use η branching fractions and uncertainties from the PDG fit [12]. As a systematic cross-check, we compare ratios of $J/\psi \rightarrow \gamma\eta$ corrected yields in different decay modes and find consistency with our previous measurement [21] and Ref. [12].

The net event yield for each channel listed in Table I is divided by its respective efficiency, intermediate decay branching fraction (from PDG [12] for η and this analysis for η'), and total number of charmonia produced. The resulting branching fractions appear in Table III, where multiple $\eta^{(\prime)}$ sub-mode values have been combined in a weighted average. For $J/\psi \rightarrow \gamma\pi^0$, $\gamma\eta$, $\gamma\eta'$, and $\psi(2S) \rightarrow \gamma\eta'$ the results are consistent with previous measurements. We set improved upper limits for $\psi(2S) \rightarrow \gamma\pi^0$ and $\gamma\eta$ and first upper limits for $\psi(3770) \rightarrow \gamma\pi^0$, $\gamma\eta$, and $\gamma\eta'$. These upper limits are computed using simulated trials in which Poisson pseudo-random numbers are thrown for background and signal levels, accounting for sideband-window-size scaling, systematic errors, and fluctuations in the observed backgrounds, in a manner similar to that in Ref. [27].

The selected $J/\psi \rightarrow \gamma\eta'$ events allow measurement of branching fractions for the five most common η' decay modes. Ratios of branching fractions follow from the $J/\psi \rightarrow \gamma\eta'$ entries in Table I and the world average value for $\mathcal{B}(\eta \rightarrow \gamma\gamma)$ [12]. The resulting ratios appear in Table IV and represent the most precise individual measurements [12]. Absolute branching fractions for these five modes can also be obtained by constraining their sum. After combining branching fractions for $\pi^+\pi^-\pi^0$ and $\pi^+\pi^-e^+e^-$ [28] with those for $3\pi^0$ and $\mu^+\mu^-\gamma$ [12], $(99.2 \pm 0.2)\%$ of all η' decays remain for the largest five decay modes. We impose this constraint, accounting for correlated systematic uncertainties, and obtain the absolute branching fractions in Table IV. The values shown are consistent with those from the PDG constrained fit [12] and of comparable precision.

In summary, we have described improved measurements of and new limits on branching fractions for charmonium decays to a photon and a light pseudoscalar meson. We also have performed the first simultaneous measurement of the five largest η' branching fractions, attaining improved precisions. Our result for $\mathcal{B}(J/\psi \rightarrow \gamma\pi^0)$ improves precision and confirms earlier central values [12], yielding a better experimental constraint [15] on the $\gamma^* \rightarrow \gamma\pi^0$ vertex in the timelike regime at $|q^2| = m^2(J/\psi)$. For the ratio of $\eta : \eta'$ production rates from each resonance we obtain $R_1 = (21.1 \pm 0.9)\%$ for J/ψ and $R_2 < 1.8\%$ at 90% C.L. for $\psi(2S)$, where for both results statistical and systematic uncertainties from the input branching

fractions from Table III have been combined in quadrature after accounting for correlations. Such a small value of R_2 is unanticipated, posing a challenge to our understanding of $c\bar{c}$ bound state decays.

We gratefully acknowledge the effort of the CESR staff in providing us with excellent luminosity and running conditions. D. Cronin-Hennessey and A. Ryd thank the A.P. Sloan Foundation. This work was supported by the National Science Foundation, the U.S. Department of Energy, the Natural Sciences and Engineering Research Council of Canada, and the U.K. Science and Technology Facilities Council.

-
- [1] J.L. Rosner, Phys. Rev. D **64**, 094002 (2001); J.L. Rosner, Annals Phys. **319**, 1 (2005).
- [2] S.B. Athar *et al.* (CLEO Collaboration), Phys. Rev. D **76**, 072003 (2007).
- [3] J.L. Rosner, Phys. Rev. D **27**, 1101 (1983); *Proceedings of the 1985 International Symposium on Lepton and Photon Interactions at High Energies, Kyoto, Japan, 1985*, edited by M. Konuma and K. Takahashi (Research Institute of Fundamental Physics, Kyoto University, Kyoto, 1986), p. 448.
- [4] F.J. Gilman and R. Kauffman, Phys. Rev. D **36**, 2761 (1987), Erratum *ibid.* D **37**, 3348 (1988).
- [5] M. Ablikim *et al.* (BES Collaboration), Phys. Rev. D **73**, 052008 (2006).
- [6] F. Ambrosino *et al.* (KLOE Collaboration), Phys. Lett. B **648**, 267 (2007).
- [7] R. Escribano and J. Nadal, J. High Energy Phys. **05**, 006 (2007).
- [8] J.Z. Bai *et al.* (BES Collaboration), Phys. Rev. D **58**, 097101 (1998).
- [9] H. Fritzsch and J.D. Jackson, Phys. Lett. B **66**, 365 (1977).
- [10] K.T. Chao, Nucl. Phys. B **335**, 101 (1990).
- [11] G.W. Intemann, Phys. Rev. D **27**, 2755 (1983).
- [12] C. Amsler *et al.* (Particle Data Group), Phys. Lett. B **667**, 1 (2008).
- [13] V.L. Chernyak and A.R. Zhitnitsky, Phys. Rep. **112**, 173 (1984).
- [14] J. Gronberg *et al.* (CLEO Collaboration), Phys. Rev. D **57**, 33 (1998).
- [15] J.L. Rosner, arXiv:0903.1796[hep-ph], (2009).
- [16] Y. Kubota *et al.* (CLEO Collaboration), Nucl. Instrum. Meth. A **320**, 66 (1992); M. Artuso *et al.*, Nucl. Instrum. Meth. A **554**, 147 (2005); D. Peterson *et al.*, Nucl. Instrum. Meth. A **478**, 142 (2002); CLEO-c/CESR-c Taskforces & CLEO-c Collaboration, Cornell University LEPP Report No. CLNS 01/1742 (2001) (unpublished).
- [17] H. Mendez *et al.* (CLEO Collaboration), Phys. Rev. D **78**, 011102 (2008).
- [18] S. Dobbs *et al.* (CLEO Collaboration), Phys. Rev. D **76**, 112001 (2007); D. Besson *et al.* (CLEO Collaboration), Phys. Rev. Lett. **96**, 092002 (2006).
- [19] D.J. Lange, Nucl. Instrum. Methods Phys. Res., Sect. A **462**, 152 (2001).
- [20] R. Brun *et al.*, Geant 3.21, CERN Program Library Long Writeup W5013 (1993), unpublished.
- [21] A. Lopez *et al.* (CLEO Collaboration), Phys. Rev. Lett. **99**, 122001 (2007).
- [22] J. Libby *et al.* (CLEO Collaboration), Phys. Rev. Lett. **101**, 182002 (2008).
- [23] J.G. Layter *et al.*, Phys. Rev. D **7**, 2565 (1973).
- [24] B. Aubert *et al.* (BABAR Collaboration), Phys. Rev. D **74**, 012002 (2006).
- [25] G. P. Lepage and S. J. Brodsky, Phys. Rev. D **22**, 2157 (1980); S. J. Brodsky and G. P. Lepage, Phys. Rev. D **24**, 1808 (1981).
- [26] N.E. Adam *et al.* (CLEO Collaboration), Phys. Rev. Lett. **96**, 082004 (2006).
- [27] G.J. Feldman and R.D. Cousins, Phys. Rev. D **57**, 3873 (1998).
- [28] P. Naik *et al.* (CLEO Collaboration), Phys. Rev. Lett. **102**, 061801 (2009).

TABLE I: For each decay mode, the number of events in the signal region (N); the total number in sideband intervals, both for meson candidate mass (S_M) and, where applicable, transition dipion recoil mass (S_J), without scale factors applied; the sum of scaled continuum and MC feedacross backgrounds (F), which is negative when scaled sidebands exceed signal counts; and the MC efficiency (ϵ).

Mode	N	S_M	S_J	F	$\epsilon(\%)$
$J/\psi \rightarrow \gamma\pi^0$	113	9	33	-2	31.1
$\rightarrow \gamma\eta(\gamma\gamma)$	1137	80	69	4	26.3
$\rightarrow \gamma\eta(3\pi^0)$	256	21	6	0	7.0
$\rightarrow \gamma\eta(\pi^+\pi^-\pi^0)$	217	5	30	0	9.0
$\rightarrow \gamma\eta(\gamma\pi^+\pi^-)$	105	62	12	-12	21.0
$\rightarrow \gamma\eta'[\pi^+\pi^-\eta(\gamma\gamma)]$	1208	36	56	3	14.2
$\rightarrow \gamma\eta'[\pi^0\pi^0\eta(\gamma\gamma)]$	245	63	16	-2	4.9
$\rightarrow \gamma\eta'(\gamma\pi^+\pi^-)$	3205	133	129	5	21.8
$\rightarrow \gamma\eta'[\gamma\omega(\pi^+\pi^-\pi^0)]$	71	18	8	0	5.6
$\rightarrow \gamma\eta'(\gamma\gamma)$	317	230	16	0	22.7
$\psi(2S) \rightarrow \gamma\pi^0$	31	89	-	-33	20.0
$\rightarrow \gamma\eta(3\pi^0)$	2	4	-	0	15.8
$\rightarrow \gamma\eta(\pi^+\pi^-\pi^0)$	1	1	-	0	12.6
$\rightarrow \gamma\eta(\gamma\pi^+\pi^-)$	1	7	-	-1	32.1
$\rightarrow \gamma\eta'[\pi^+\pi^-\eta(\gamma\gamma)]$	120	3	-	0	22.6
$\rightarrow \gamma\eta'[\pi^0\pi^0\eta(\gamma\gamma)]$	46	39	-	0	11.2
$\rightarrow \gamma\eta'(\gamma\pi^+\pi^-)$	343	91	-	1	35.3
$\rightarrow \gamma\eta'[\gamma\omega(\pi^+\pi^-\pi^0)]$	12	6	-	-1	9.9
$\psi(3770) \rightarrow \gamma\pi^0$	331	1396	-	-468	19.8
$\rightarrow \gamma\eta(3\pi^0)$	9	0	-	0	19.4
$\rightarrow \gamma\eta(\pi^+\pi^-\pi^0)$	7	1	-	0	23.2
$\rightarrow \gamma\eta'[\pi^+\pi^-\eta(\gamma\gamma)]$	8	1	-	0	33.9
$\rightarrow \gamma\eta'[\pi^+\pi^-\eta(3\pi^0)]$	3	0	-	0	7.3
$\rightarrow \gamma\eta'[\pi^+\pi^-\eta(\pi^+\pi^-\pi^0)]$	5	0	-	0	13.5

TABLE II: Mass windows and sideband (SB) intervals in MeV.

Mode	Window	Lower SB	Upper SB
$\pi^+\pi^-$ -recoil	3087-3107	2980-3080	3114-3214
$\pi^0 \rightarrow \gamma\gamma$	110-160	50-100	170-220
$\eta \rightarrow \gamma\pi^+\pi^-$	535-560	460-510	585-635
\rightarrow other modes	500-580	400-480	600-680
$\eta' \rightarrow \gamma\gamma, \pi^0\pi^0\eta$	920-995	730-880	1035-1185
\rightarrow other modes	945-970	890-940	975-1025
$\omega \rightarrow \pi^+\pi^-\pi^0$	750-814	-	-

 TABLE III: Branching fractions from this analysis, showing statistical and systematic uncertainties, respectively, and PDG [12]. The rightmost column shows the difference between the two in units of standard error (σ). Upper limits are quoted at 90% C.L. Entries in the last two rows include the effects of estimated continuum background and ignore (include) maximal destructive interference between $\psi(3770)$ and continuum sources.

Mode	This result (10^{-4})	PDG (10^{-4})	$\#\sigma$
$J/\psi \rightarrow \gamma\pi^0$	$0.363 \pm 0.036 \pm 0.013$	$0.33^{+0.06}_{-0.04}$	0.4
$\rightarrow \gamma\eta$	$11.01 \pm 0.29 \pm 0.22$	9.8 ± 1.0	1.2
$\rightarrow \gamma\eta'$	$52.4 \pm 1.2 \pm 1.1$	47.1 ± 2.7	1.7
$\psi(2S) \rightarrow \gamma\pi^0$	< 0.05	< 54	-
$\rightarrow \gamma\eta$	< 0.02	< 0.9	-
$\rightarrow \gamma\eta'$	$1.19 \pm 0.08 \pm 0.03$	1.36 ± 0.24	-0.7
$\psi(3770) \rightarrow \gamma\pi^0$	< 2	-	-
$\rightarrow \gamma\eta$	< 0.2 (1.5)	-	-
$\rightarrow \gamma\eta'$	< 0.2 (1.8)	-	-

 TABLE IV: Relative and absolute branching fractions for η' decays from this analysis, showing statistical and systematic uncertainties.

Mode	$\mathcal{B}/\mathcal{B}(\pi^+\pi^-\eta)$ (%)	\mathcal{B} (%)
$\pi^+\pi^-\eta$	$\equiv 100$	$42.4 \pm 1.1 \pm 0.4$
$\pi^0\pi^0\eta$	$55.5 \pm 4.3 \pm 1.3$	$23.5 \pm 1.3 \pm 0.4$
$\gamma\pi^+\pi^-$	$67.7 \pm 2.4 \pm 1.1$	$28.7 \pm 0.7 \pm 0.4$
$\gamma\omega$	$5.5 \pm 0.7 \pm 0.1$	$2.34 \pm 0.30 \pm 0.04$
$\gamma\gamma$	$5.3 \pm 0.4 \pm 0.1$	$2.25 \pm 0.16 \pm 0.03$

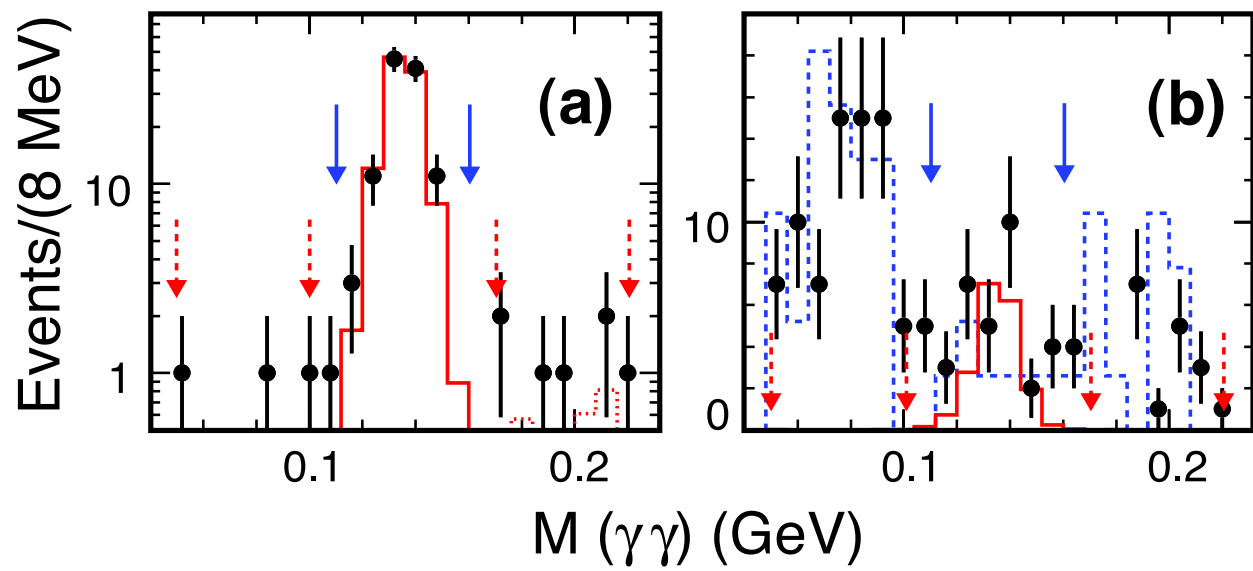


FIG. 1: Two-photon mass distributions for $\gamma\pi^0$ final states from (a) J/ψ and (b) $\psi(2S)$. Points show the $\psi(2S)$ data; dashed histogram, the luminosity-scaled continuum data; solid line histogram, signal MC; and dotted histogram, MC feedacross from other γP decays. Upper solid arrows show nominal selection criteria; all selection criteria are in place except those upon plotted mass. Lower dashed arrows show sidebands.

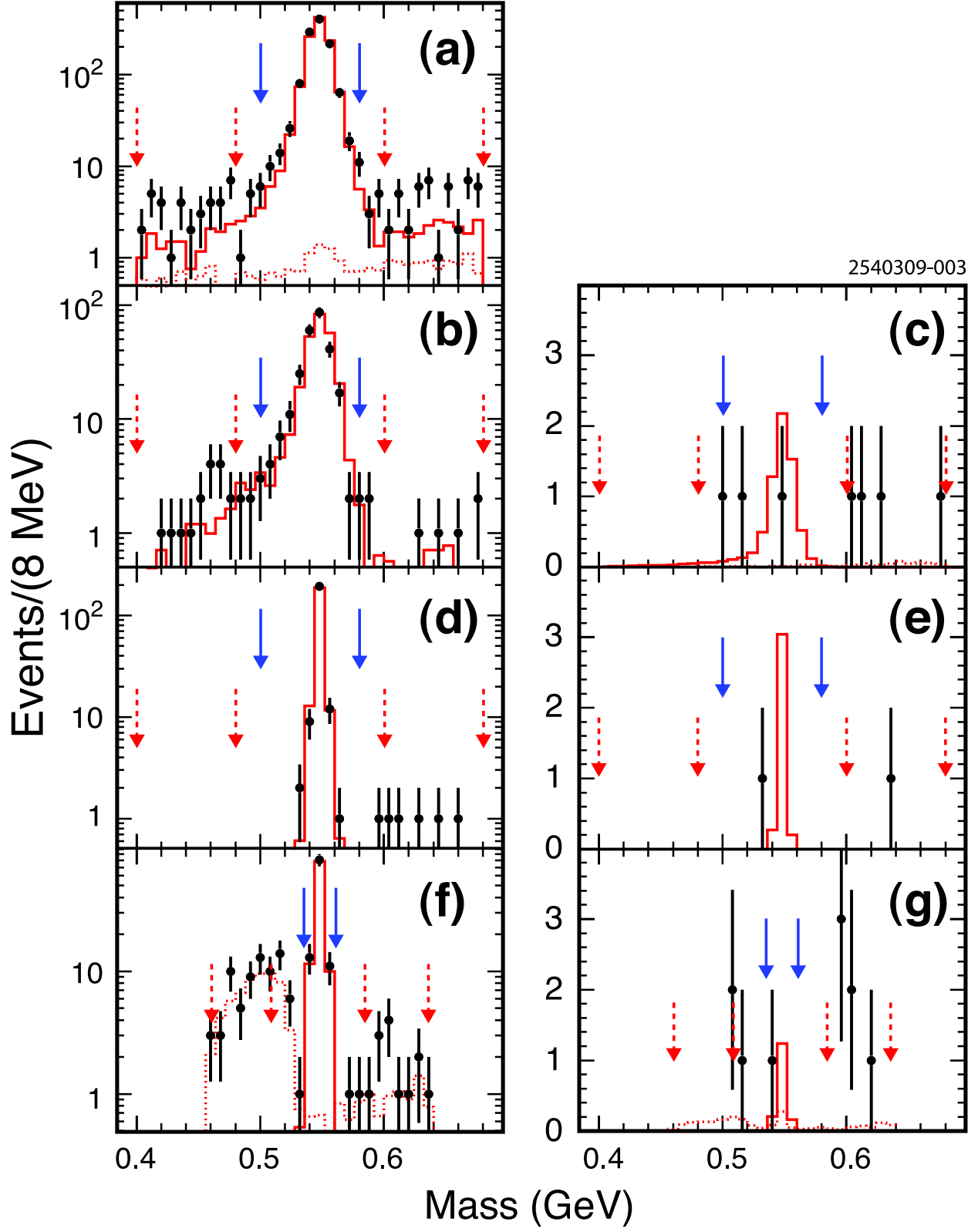


FIG. 2: Distributions of η candidate mass for $\gamma\eta$ final states from J/ψ (left) and $\psi(2S)$ (right). The η decay modes are (a) $\gamma\gamma$; (b), (c) $3\pi^0$; (d), (e) $\pi^+\pi^-\pi^0$; and (f), (g), $\gamma\pi^+\pi^-$. Symbols are defined in Fig. 1.

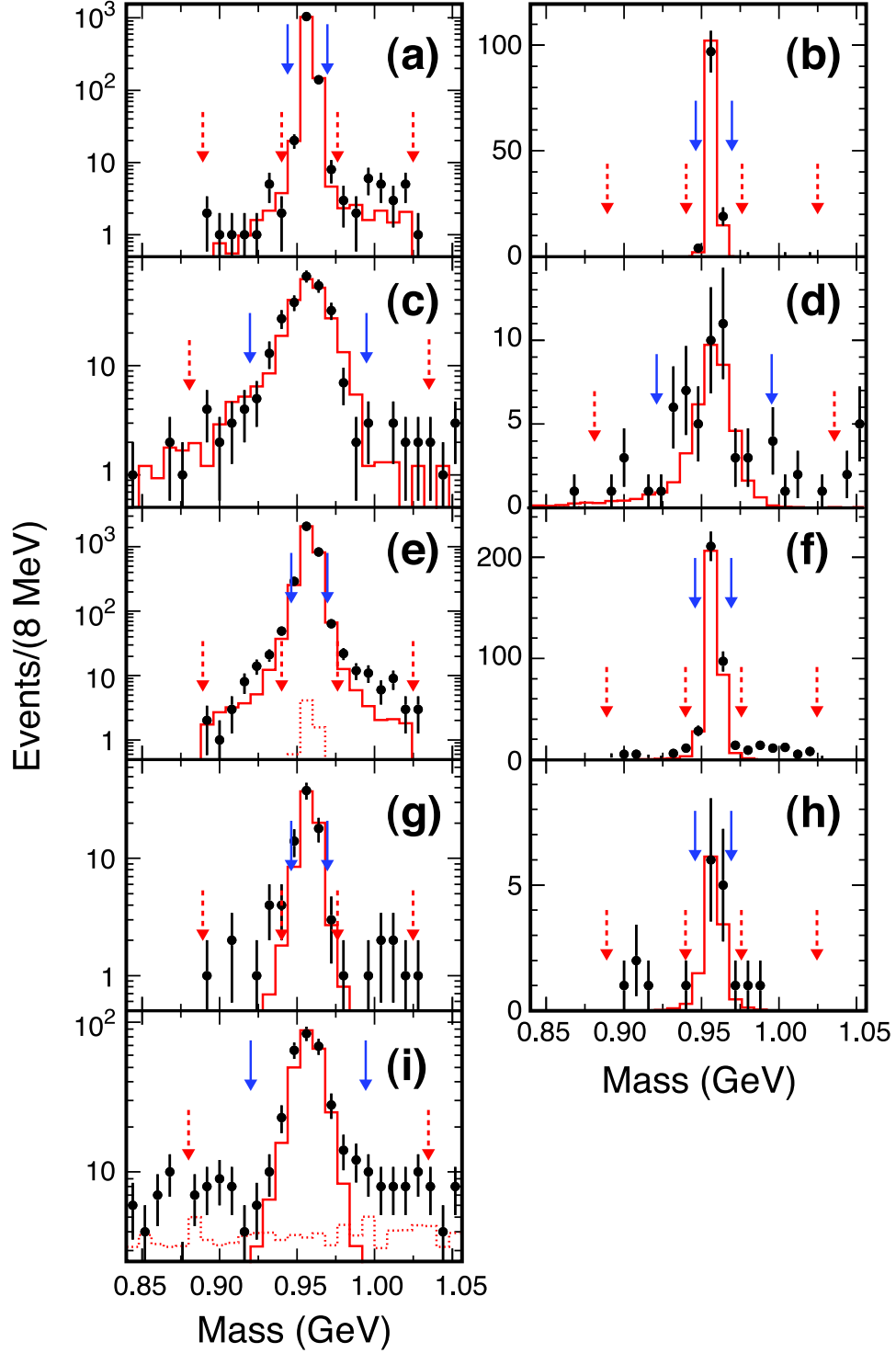


FIG. 3: Distributions of η' candidate mass for $\gamma\eta'$ final states from J/ψ (left) and $\psi(2S)$ (right). The η' decay modes are (a), (b) $\pi^+\pi^-\eta(\gamma\gamma)$; (c), (d) $\pi^0\pi^0\eta(\gamma\gamma)$; (e), (f) $\gamma\pi^+\pi^-$; (g), (h) $\gamma\omega(\pi^+\pi^-\pi^0)$; and (i) $\gamma\gamma$. Symbols are defined in Fig. 1. In (c), (d), and (i), only parts of the sideband intervals are shown.

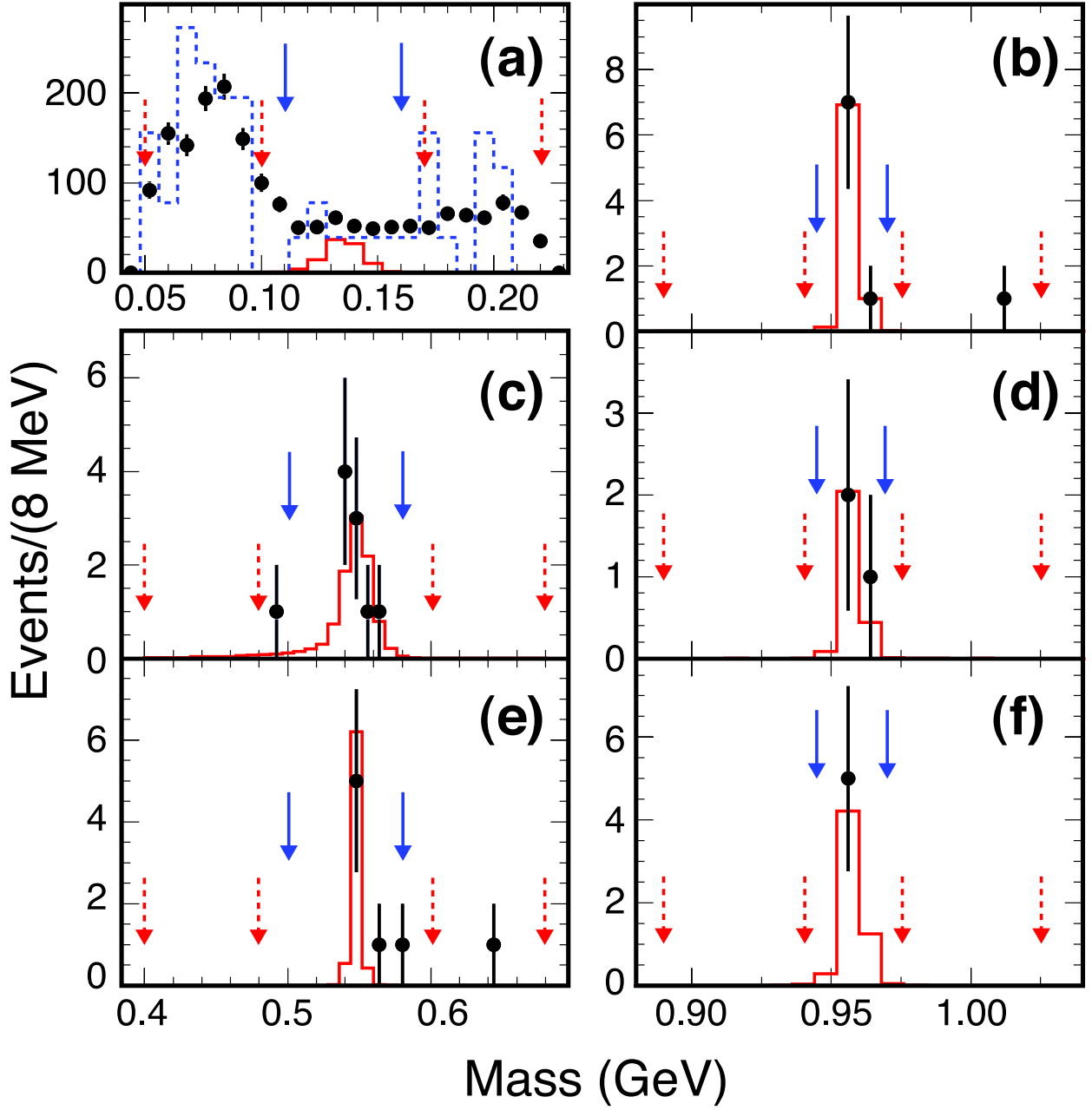


FIG. 4: Distributions of light quark meson candidate mass for $\sqrt{s} = 3.773$ GeV final states of (a) $\gamma\pi^0$; (c), (e) $\gamma\eta$; and (b), (d), (f) $\gamma\eta'$. Decay modes are (b) $\gamma\eta'[\pi^+\pi^-\eta(\gamma\gamma)]$, (c) $\gamma\eta(3\pi^0)$, (d) $\gamma\eta'[\pi^+\pi^-\eta(3\pi^0)]$, (e) $\gamma\eta(\pi^+\pi^-\pi^0)$, and (f) $\gamma\eta'[\pi^+\pi^-\eta(\pi^+\pi^-\pi^0)]$. Symbols are defined in Fig. 1.